

Interface control and snow crystal growth

Jessica Li

Harvard University, Cambridge, Massachusetts 02138, United States

Laura P. Schaposnik

University of Illinois, Chicago, Illinois 60607, United States

(Received 18 June 2015; published 8 February 2016)

The growth of snow crystals is dependent on the temperature and saturation of the environment. In the case of dendrites, Reiter's local two-dimensional model provides a realistic approach to the study of dendrite growth. In this paper we obtain a new geometric rule that incorporates interface control, a basic mechanism of crystallization that is not taken into account in the original Reiter model. By defining two new variables, growth latency and growth direction, our improved model gives a realistic model not only for dendrite but also for plate forms.

DOI: [10.1103/PhysRevE.93.023302](https://doi.org/10.1103/PhysRevE.93.023302)

I. INTRODUCTION

Snowflake growth is a specific example of crystallization: how crystals grow and create complex structures. Because crystallization corresponds to a basic phase transition in physics, and crystals make up the foundation of several major industries, studying snowflake growth helps gaining understanding of how molecules condense to form crystals. This fundamental knowledge may help fabricate novel types of crystalline materials [1].

Snowflakes exhibit a rich combination of characteristic symmetry and complexity. The sixfold symmetry is a result of the hexagonal structure of the ice crystal lattice, and the complexity comes from the random motion of individual snow crystals falling through the atmosphere (see Fig. 1).

Scientific studies of snowflakes can be categorized into two main types. The first approach takes a macroscopic view by observing natural snowflakes in a variety of morphological environments characterized by temperature, pressure, and vapor density (e.g., Refs. [3–5]). The second type takes a microscopic view and investigates the basic physical mechanisms governing the growth of snowflakes (e.g., see Ref. [1]). While some aspects of snowflake growth (e.g., the crystal structure of ice) are well understood, many other aspects such as diffusion limited growth are at best understood at a qualitative level [1].

Another approach in which snowflake growth is numerically simulated to produce images with mathematical models derived from physical principles is through computer modeling (e.g., see Refs. [6–11]). By comparing computer generated images with actual snowflakes, one can correlate the mathematical models and their parameters with physical conditions. While computer modeling can generate snowflake images that successfully capture some basic features of actual snowflakes, certain fundamental features of snowflake growth are not well understood, and so far there has been only limited analysis of these computer models in the literature (e.g., Refs. [6,7,12–14] and references therein). One of the key challenges has been that the snowflake growth models consist of a large set of PDEs, and as in many chaos theoretic problems, rigorous study is difficult.

In this paper we analyze snowflake growth simulated by the computer models. The models that have been considered

in the past are in essence chaos theoretic models, which is why they successfully capture the real world phenomena but prove to be notoriously difficult to analyze rigorously. In particular, two mechanisms studying the instability of the crystal have been studied in the past: the Mullins-Sekerka instability, and the facet instability for a hexagonal prism snow crystal (e.g., see Refs. [12,15] and references therein). Some models, e.g., proposed in Refs. [6,7,13], are highly detailed and sophisticated and meant to almost exactly match snow crystal growth, while others, e.g., Reiter's model [10], are relatively simple meant for understanding, thought experiments and analysis. In this paper we study Reiter's model using a combined approach of mathematical analysis and numerical simulation. It should be pointed out that the goal of this paper is to provide mathematical treatment of the computational model. The model, however, is an artificial one and does not include the actual growth processes. As such, the paper is not intended to further the understanding the formation mechanism of actual snowflake patterns.

After reviewing Reiter's model in Sec. II, in Sec. III we divide a snowflake image into main branches and side branches and define two new variables (growth latency and growth direction) to characterize the growth patterns. In Sec. IV we derive a closed form solution of the main branch growth latency using a one-dimensional linear model and compare it with the simulation results using the hexagonal automata. Then in Sec. V we discover a few interesting patterns of the growth latency and direction of side branches. On the basis of the analysis and the principle of surface free energy minimization, in Sec. VI we enhance Reiter's model and thus obtain realistic results both for dendrites and plate forms. We summarize our contributions and present a few future work directions in Sec. VII.

II. AN OVERVIEW OF REITER'S MODEL

Reiter's model is a hexagonal automata which can be described as follows. Given a tessellation of the plane into hexagonal cells, each cell z has six nearest neighbors. We shall denote by $s_t(z) \in \mathbb{R}_{>0}$ the state variable of cell z at time



FIG. 1. Examples of real plate and dendrite snowflakes [2]. (a) Stellar dendrite, (b) stellar plate, (c) sectored plate.

t which gives the amount of water stored in z . Then cells are divided into three types.

Definition 1. A cell z is frozen if $s_t(z) \geq 1$ (an F cell). If a cell is not frozen itself but at least one of the nearest neighbors is frozen, the cell is a boundary cell (a B cell). A cell that is neither frozen nor boundary is called nonreceptive (an NR cell). The union of frozen and boundary cells are called receptive cells (R cells; Fig. 2).

The initial condition in Reiter's model is

$$s_0(z) = \begin{cases} 1 & \text{if } z = \mathcal{O} \\ \beta & \text{if } z \neq \mathcal{O} \end{cases}$$

where \mathcal{O} is the origin cell, and β represents a fixed constant *background vapor level*.

Definition 2. Define the following functions on a cell z : the amount of water that participates in diffusion $u_t(z)$, and the amount of water that does not participate $v_t(z)$. Hence,

$$s_t(z) = u_t(z) + v_t(z), \quad (1)$$

and we let $v_t(z) := s_t(z)$ if z is receptive, and $v_t(z) := 0$ if z is nonreceptive.

For γ, α , two fixed constants representing *vapor addition* and *diffusion coefficients*, respectively, in Reiter's model, the state of a cell evolves as a function of the states of its nearest neighbors according to two local update rules that reflect the underlying mathematical models:

(1) *Constant addition.* For any receptive cell z ,

$$v_t^+(z) := v_t^-(z) + \gamma. \quad (2)$$

(2) *Diffusion.* For any cell z ,

$$u_t^+(z) := u_t^-(z) + \frac{\alpha}{2} [\bar{u}_t^-(z) - u_t^-(z)], \quad (3)$$

where we have used upper indices \pm to denote new functions giving the state variable of a cell before and after a step is completed and written $\bar{u}_t^-(z)$ for the average of u_t^- for the six nearest neighbors of cell z .

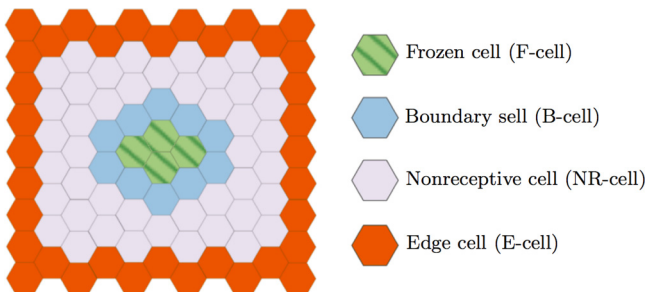


FIG. 2. Classification of cells.

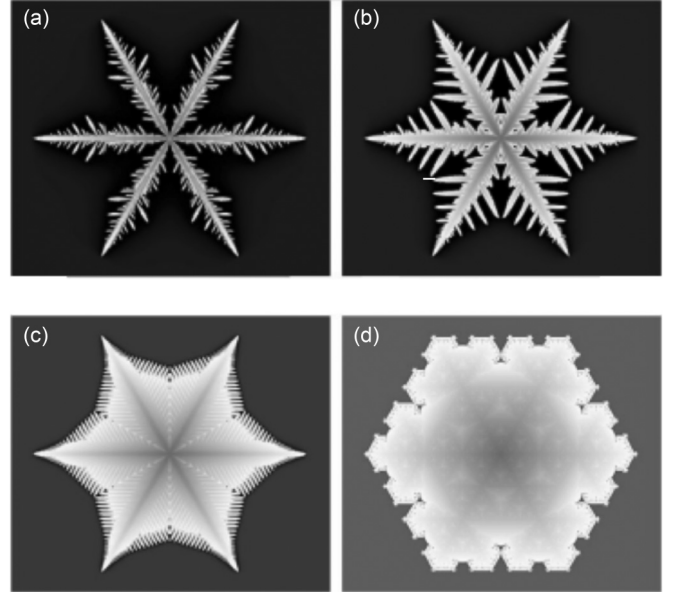


FIG. 3. Images generated by Reiter's model [10] for $\alpha = 1$ and parameters (a) $\beta = 0.3, \gamma = 0.0001$; (b) $\beta = 0.35, \gamma = 0.001$; (c) $\beta = 0.6, \gamma = 0.01$; (d) $\beta = 0.9, \gamma = 0.05$.

The underlying physical principle of Eq. (3) is the diffusion equation

$$\partial u / \partial t = a \nabla^2 u, \quad (4)$$

where a is a constant. Indeed, Eq. (3) is the discrete version of Eq. (4) on the hexagonal lattice, and it states that a cell z retains $(1 - \alpha/2)$ fraction of $u_t^-(z)$, uniformly distributes the remaining to its six neighbors, and receives $\alpha/12$ fraction from each neighbor. The total amount of $u_t(z)$ would be conserved within the entire system, except that a real world simulation consists of a finite number of contiguous cells. The cells at the edge of the simulation setup are referred to as *edge cells*, in which one sets $u_t^+(z) := \beta$. Thus, water is added to the system via the edge cells in the diffusion process. Combining the two intermediate variables, one obtains

$$s_{t+1}(z) := u_t^+(z) + v_t^+(z). \quad (5)$$

By varying the parameters α, β, γ in Reiter's model one can generate certain geometric forms of snowflakes observed in nature (Fig. 3).

III. GENERAL GEOMETRIC PROPERTIES

In what follows, we give new descriptions of snowflake growth and analyze them with a combined approach of mathematical analysis and numerical simulation by considering a coordinate system of cells as in Fig. 4(a). A cell z is represented by its coordinate (i, j) , for $i, j \in \mathbb{Z}$, with the origin $\mathcal{O} = (0, 0)$. Since there is a sixfold symmetry, we focus on only one-twelfth of the cells, marked as dark dots, for which $j \geq i \geq 0$:

The images in Fig. 3 show that a crystal consists of six main branches that grow along the lattice axes, and numerous side branches that grow from the main branches in a seemingly random manner. The main and side branches exhibit a rich combination of characteristic symmetry and complexity which

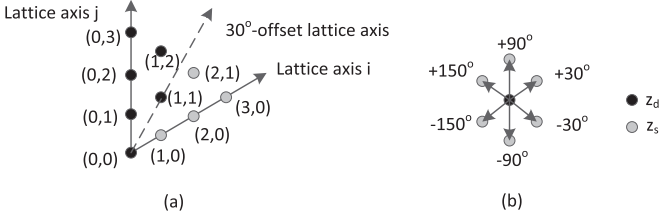


FIG. 4. (a) Coordinate system of hexagonal cells. (b) Definition of growth directions in the coordinate system.

we shall study through the rate of water accumulation of a cell z , defined by

$$\Delta s_t(z) = s_{t+1}(z) - s_t(z).$$

At any time the set of all the R cells is connected. Moreover since a frozen cell is surrounded by receptive cells and does not accumulate water via diffusion, and since water flows from nonreceptive cells to boundary cells, one has that the rate of water accumulation $\Delta s_t(z)$ of a cell satisfies the following general geometric properties:

(A) For an NR cell z , one has $0 < s_t(z) \leq \beta$ and $\Delta s_t(z) \leq 0$. Suppose that an NR cell z is surrounded by R cells and disconnected from the E cells. If $\gamma > 0$, there exists $t_0 > 0$ such that $s_{t_0}(z) \geq 1$ (i.e., a time t_0 in which the cell becomes frozen); otherwise the NR cell will permanently remain nonreceptive and never become frozen.

(B) For a B cell z the quantity $\Delta s_t(z)$ is the sum of γ and diffusion. If $\gamma > 0$, there exists $t_0 > 0$ such that $s_{t_0}(z) \geq 1$; otherwise, if cell z is surrounded by a set of F cells and disconnected from the E cells, then as in (A), the cell will never become frozen:

$$\lim_{t \rightarrow \infty} s_t(z) < 1.$$

(C) For an F cell z , one has $\Delta s_t(z) = \gamma$.

(D) The state variable is $s_t(z) = \beta$ only for z an E cell.

Thus, for an NR cell to become frozen, the cell goes through two stages of growth. First, the NR cell loses vapor to other cells due to diffusion, as in (A). Subsequently, it becomes a B cell and accumulates water via diffusion and addition, as in (B), until it becomes frozen and sees no benefit of diffusion, as in (C). Becoming a B cell is a critical event between the two stages.

We focus on the second stage and define two new variables to characterize growth patterns.

Definition 3. The time to be frozen of a cell z is denoted by $T(z)$ and defined by the condition $s_{T(z)}(z) \geq 1$, and $s_t(z) < 1$ for $t < T(z)$. Similarly, we define $B(z)$ as the first time to be boundary. Finally, growth latency is denoted by $L(z)$ and defined by $L(z) := T(z) - B(z)$.

A cell becomes a B cell as one of its neighboring cells has just become an F cell, and thus it is useful to make the following definition in terms of redistribution of water.

Definition 4. Denote by z_d a destination cell, and by z_s a source cell. Then the growth direction of cell z_d is denoted by $g(z_d)$ and defined as the orientation of z_s with respect to z_d , where the angle is with respect to the horizontal axis. The source-destination cell relationship shall be denoted by $S(z_d) := z_s$.

As shown in Fig. 4(b), the angle is given relative to the horizontal direction in the coordinate system and satisfies

$$g(z_d) \in \{+30^\circ, -30^\circ, +90^\circ, -90^\circ, +150^\circ, -150^\circ\}.$$

Note that while the growth of z_d is traced back to a unique z_s , a source cell may correspond to multiple destination cells.

IV. GROWTH OF MAIN BRANCHES

Consider cells (i, j) where $i + j = K$ for a fixed K . These cells are all K sites away from the origin $(0, 0)$ on the grid. The main branch growth pattern is such that $T(0, K) \leq T(i, j)$ and

$$T\left(\frac{K}{2}, \frac{K}{2}\right) \geq T(i, j) \quad \text{for even } K,$$

$$T\left(\frac{K-1}{2}, \frac{K-1}{2}\right) \geq T(i, j) \quad \text{for odd } K.$$

Along the lattice j axis, one has $g(0, j) = -90^\circ$ for all j . Hence, the snowflake growth is fastest along a lattice axis, which represents a main branch, and is the slowest along the 30° -offset lattice axis.

We next develop a model to calculate the growth latency $L(0, j)$. As cell $(0, j)$ becomes frozen, cell $(0, j + 1)$ becomes a boundary cell. Hence the first time to be boundary $B(0, j + 1) = T(0, j)$, and thus one can calculate $T(0, j)$ as

$$T(0, j) = T(0, 0) + \sum_{k=1}^j L(0, k). \quad (6)$$

In order to gain analytical understanding, we first study a one-dimensional model. Consider a line of consecutive cells z_0, z_1, \dots, z_N , where z_N is the edge cell. Initially cell \mathcal{O} is frozen. We focus on the growth period $[B(k), T(k)]$ in which cells z_0, z_1, \dots, z_{k-1} are frozen and cell k grows from boundary to frozen. Since Eq. (3) describes the diffusion dynamics of vapor being transferred from the edge cell to cell z_k , and cell z_k accumulates water via addition [Eq. (2)], to derive an analytical solution, we make the following assumption which we justify shortly.

Assumption 1. For $t \in [B(z_k), T(z_k)]$, assume that in Eq. (3) one has

$$u_t^+(z_i) = u_t^-(z_i),$$

for $k + 1 \leq i \leq N$, for N as above and $B(z_k), T(z_k)$ as in Definition III. Therefore, the vapor distribution reaches a steady state, denoted as $\mu(i|k)$.

From Assumption IV, we can ignore the notations of \pm , and reduce Eq. (3) to the linear equation

$$\mu(i|k) = \frac{1}{2} [\mu(i-1|k) + \mu(i+1|k)]. \quad (7)$$

Moreover, with the boundary conditions $\mu(k|k) = 0$ and $\mu(N|k) = \beta$, the vapor distribution can be written in a closed form as follows:

$$\mu(i|k) = \frac{i-k}{N-k} \beta, \quad \text{for } i = k, \dots, N, \quad (8)$$

which graphically represents a line that connects the two boundary condition points.

We shall now explain why Assumption IV is well motivated. Suppose that the steady state distribution Eq. (8) is already

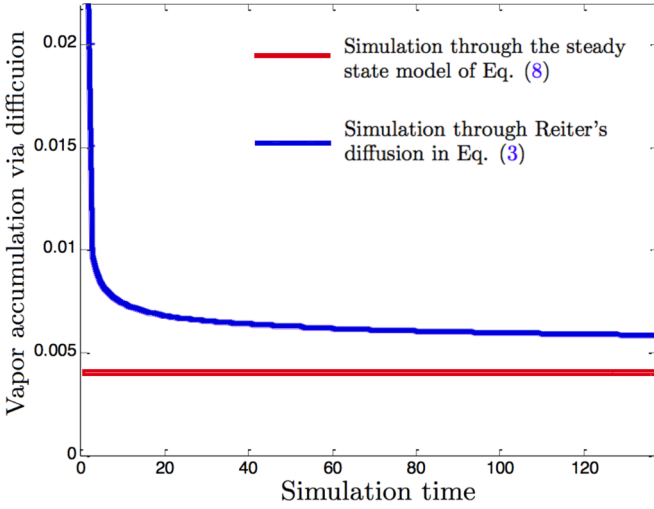


FIG. 5. Comparison of vapor accumulation simulations for the parameters $\alpha = 1, \beta = 0.4, \gamma = 0.001$.

reached at $t = B(z_k)$:

$$s_{B(z_k)}(z_i) = \mu(i|k-1) = \frac{i - (k-1)}{N - (k-1)}\beta \quad \text{for } i = k, \dots, N.$$

Then $s_t(z_i)$ evolves in the interval of $(B(z_k), T(z_k)]$ in the following manner. For $N \gg k$, one has

$$s_{B(z_k)}(z_k) = \mu(k|k-1) = \frac{1}{(N-k+1)}\beta \approx 0.$$

Thus it is reasonable to assume

$$L(z_k) = T(z_k) - B(z_k) \gg 1$$

because cell z_k will take several simulation steps to reach $s_{T(z_k)}(z_k) \geq 1$. Moreover,

$$|s_{B(z_k)}(z_i) - \mu(i|k)| = \left| \frac{i - (k-1)}{N - (k-1)}\beta - \frac{(i-k)}{(N-k)}\beta \right| \ll 1$$

for $N \gg k$. Thus, in each simulation step for time $t \in (B(z_k), T(z_k)]$, the function $s_t(z_i)$ varies only slightly and can be considered approximately constant. Hence, $u_t^+(z_i) = u_t^-(z_i)$.

From Eq. (3) and Eq. (7), we may estimate $u_t^+(z_k)$ by

$$\hat{u}_t^+(z_k) := \frac{\alpha}{4} \frac{1}{N-k} \beta.$$

Moreover, since $u_t^-(z_k) = 0$ it follows that we can further estimate $\Delta s_t(z_k)$ and $L(z_k)$ by

$$\Delta \hat{s}_t(z_k) := \frac{\alpha}{4} \frac{1}{N-k} \beta + \gamma, \quad (9)$$

$$\hat{L}(z_k) := \frac{1 - s_{B(z_k)}(z_k)}{\Delta \hat{s}_t(z_k)} = \frac{1 - \frac{1}{N-k+1}\beta}{\frac{\alpha}{4} \frac{1}{N-k} \beta + \gamma}. \quad (10)$$

In the one-dimensional model with $N = 50$, we may compare the vapor accumulation in every simulation step, as the simulation proceeds from the time when cell $k = 25$ just becomes the boundary to the time when it becomes frozen. Figure 5 compares $\Delta s_t(z_k)$ at cell z_k determined by the simulation, and $\Delta \hat{s}_t(z_k)$ predicted by Eq. (9) for time

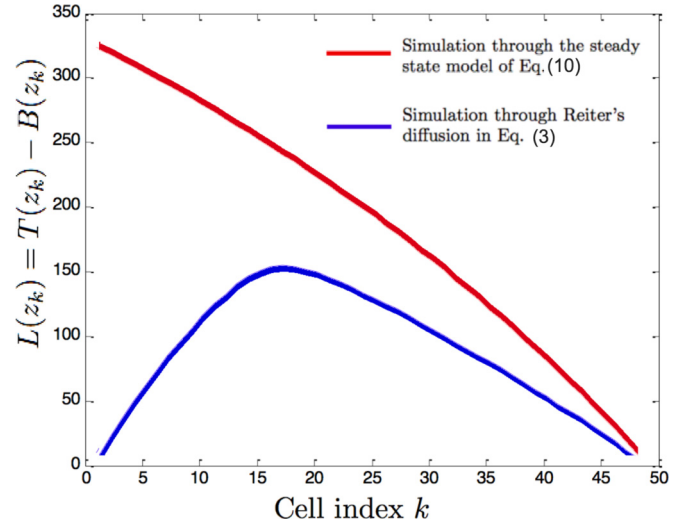


FIG. 6. Comparison of growth latency simulations for the parameters $\alpha = 1, \beta = 0.4, \gamma = 0.001$.

$t \in [B(z_k), T(z_k)]$. Initially $s_t(k) \ll \mu(i|k)$ and $\Delta s_t(k) \gg \Delta \hat{s}_t(k)$. After about five simulation steps, $\Delta s_t(k)$ drops to a flat plateau, which is approximately equal to $s_t(k)$. At any time t , one observes that $\Delta \hat{s}_t(k) \leq \Delta s_t(k)$.

One may also model $L(z_k) = T(z_k) - B(z_k)$ as a function of cell index of the cells. In the one-dimensional model with $N = 50$, Fig. 6 compares $L(k)$ determined by the simulation, and $\hat{L}(z_k)$ predicted by Eq. (10) as the snowflake grows from the origin \mathcal{O} to the edge cell. For any k , one observes that $L(z_k) < \hat{L}(z_k)$. This phenomenon is expected, since by solving the above PDEs one has that there exists $\alpha > 0$ such that at any time instance $t \in [B(z_k), T(z_k)]$, for $i = k, \dots, N$, one has

$$\mu(i|k) \leq s_t(z_i) \text{ and } \Delta \hat{s}_t(z_k) \leq \Delta s_t(z_k).$$

As a result, $\hat{L}(z_k) \geq L(z_k)$.

Equation (10) predicts that $\hat{L}(z_k)$ drops monotonically with k . In simulation, we observe that in the beginning the cells grow from boundary to frozen very quickly, well before the steady state is reached. As a result, the steady state Assumption IV does not hold in that time period. Figure 6 shows that $L(z_k)$ first increases, then drops, and eventually matches the prediction $\hat{L}(z_k)$.

Finally, we return to the two-dimensional hexagonal cellular case. With a similar steady state assumption, we can reduce the PDE to a set of linear equations similar to Eq. (7). However, the geometric structure is much more complex than the one-dimensional case. As a result, it is difficult to derive a closed form formula of the vapor distribution similar to Eq. (8).

Figure 7 plots $L(0, j)$ along a main branch. Comparison with Fig. 6 indicates a similarity between the one-dimensional and two-dimensional cases in that $L(z)$ increases as the snowflake grows from the origin. However, in the two-dimensional case, we observe from simulations that $L(0, 10) = L(0, 11) = \dots = L(0, 195)$. When the snowflake grows close to the edge cell, it experiences some edge effect in the simulation where L drops drastically. This indicates that

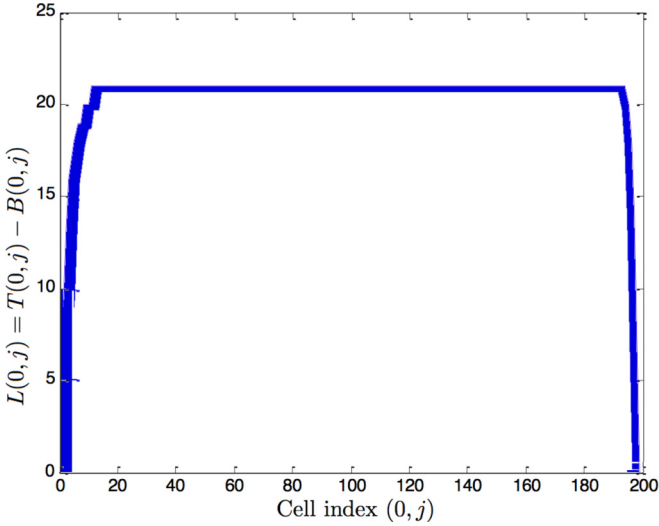


FIG. 7. $T(0, j) - B(0, j)$ of cells $(0, j)$ along a main branch for $j = 1, 2, \dots$, in the two-dimensional scenario. Here cell $(0, 200)$ is an edge cell, and $\alpha = 1$, $\beta = 0.4$, $\gamma = 0.001$.

somewhat surprisingly $\Delta s_l(0, j)$ remains almost constant as the snowflake grows along the main branch.

V. GROWTH OF SIDE BRANCHES

While the main branches of snowflakes represent clean sixfold symmetry, the side branches exhibit characteristic features of chaotic dynamics: complexity and unpredictability. Reiter's model is completely deterministic with no noise or randomness involved, and yet the resultant snowflake images are sensitive to the parameters α, β , and γ in a chaotic manner. Chaos may appear to be the antithesis of symmetry and structure. Our goal in this section is to discover growth patterns that emerge from seemingly chaotic dynamics.

Definition 5. Starting from a cell z_0 on the j -axis main branch, the set of consecutive frozen cells in the i -axis direction are referred to as side branch from cell z_0 . We shall denote by $z_E(z_0)$ the outmost cell or tip, by $E(z_0)$ the length of the side branch, and the side branch itself by $\Phi(z_0) := \{z_0, \dots, z_E(z_0)\}$.

In what follows, we study the growth latency of side branches. Figure 8 plots the tips of the side branches that grow from the j -axis main branch using the parameters of the four images in Fig. 3.

Due to the chaotic dynamics, the lengths of the side branches vary drastically with z_0 in a seemingly random manner. For image (a), most of the side branches are short and only a small number stand out. The opposite holds for image (d). The scenarios are in between for images (b) and (c). The length of the side branches is indicative of the growth latency. The long side branches represent the ones that grow fastest. In Fig. 8 we connect the tips of the long side branches to form an *envelope curve* that represents the frontier of the side branch growth. The most interesting observation is that the envelope curve can be closely approximated by a straight line for the most part. Recall that the growth latency of the main branch is a constant. Thus we infer that the growth latency of the long side branches is also constant. Denoting by L_M and L_S the *growth latencies* of the main and long side branches,

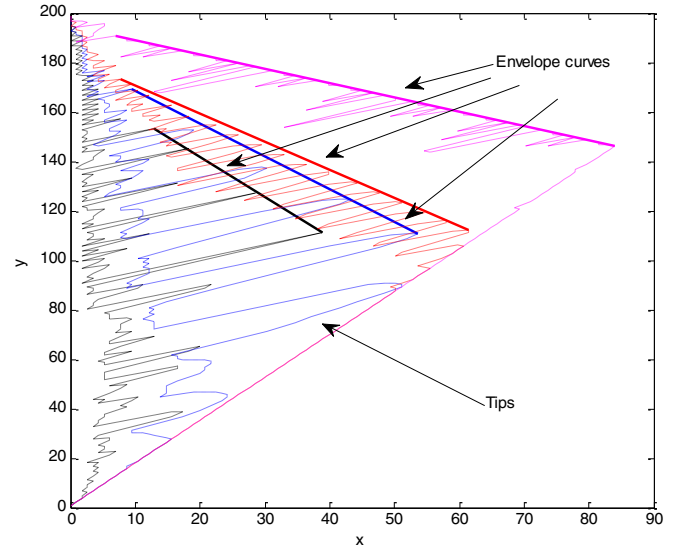


FIG. 8. Plots of the tips (thin curves) and envelope curves (thick curves) of the side branches from the j -axis main branch using the parameters of the four example images in Fig. 3. Due to symmetry, we focus on one set of side branches that grow from the right side of lattice j axis. Here the black curve represents Fig. 3(a), blue for Fig. 3(b), red for Fig. 3(c), and magenta for Fig. 3(d). The axes are the horizontal and vertical axes.

respectively, one has that

$$\frac{L_M}{L_S} = \frac{\sin 2\pi/3 - \theta}{\sin \theta}, \quad (11)$$

where θ is the angle between the envelope curve straight line and the j axis. As a specific example, for the magenta curve, the envelope curve of the long side branches grows almost as fast as the main branch, such that $\theta \approx \pi/3$ and the resultant image, appearing in Fig. 3(d), is roughly a hexagon.

We shall consider next the growth directions of the cells on side branches. Figure 9 plots the trace of the growth direction $g(z)$ (see Definition III) as a snowflake develops in the simulation. The corresponding snowflake image is shown in Fig. 3(b). When a cell z becomes boundary, we mark the cell to indicate $g(z)$ using the legend labeled in the figure. If a cell never becomes boundary, no mark is made. All side branches grow from the j -axis main branch, starting in the direction parallel to the i axis. Subsequently, a side branch may split into multiple directions. Indeed, all six orientations have been observed and the dynamics appear chaotic as $g(z)$ appears unpredictable. However, we do find an interesting pattern described below.

Definition 6. A straight path from a cell z_0 on the j -axis main branch is the set of consecutive frozen cells in the i -axis direction satisfying $z_{i-1} = S(z_i)$. The number of consecutive cells satisfying $z_{i-1} = S(z_i)$ is the length $F(z_0)$. We then denote a straight path from a cell z_0 by $\Psi(z_0) := \{z_0, z_1, z_2, \dots, z_{F(z_0)}\}$.

Comparison between Definition V and Definition V shows that the paths are nested, i.e., $\Psi(z_0) \subset \Phi(z_0)$, and hence the lengths satisfy $F(z_0) \leq E(z_0)$. When a cell z_{i-1} on the straight path becomes frozen, it triggers not only z_i in the i -axis direction but also other neighbors to become boundary,

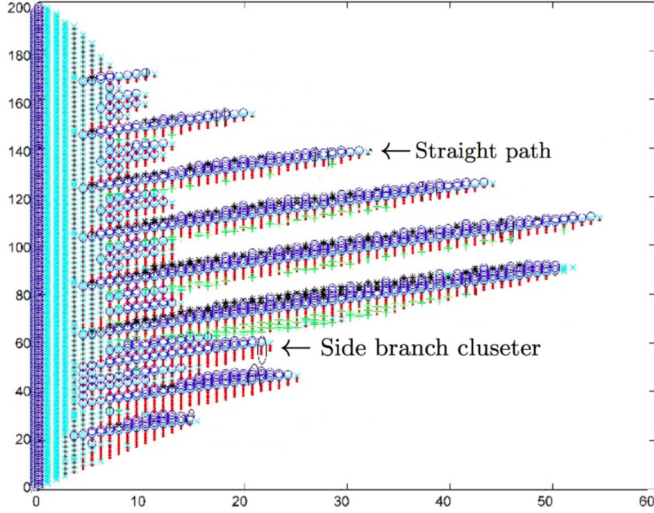


FIG. 9. Trace of relative orientations of source cells with respect to destination cells. A destination cell becomes boundary because a source cell, which is one of the neighbors of the destination cell, becomes frozen. Legend is as follows: magenta \blacksquare : $+30^\circ$, black \star : -30° , green $+$: $+90^\circ$, blue \circ : -90° , red \cdot : $+150^\circ$, cyan \times : -150° , where the parameters are $\alpha = 1, \beta = 0.35, \gamma = 0.001$. Note that not all straight paths are labeled. The axes are as in Fig. 4(a).

resulting in growth in other directions, which we call *deviating paths*. The straight and deviating paths collectively form a *side branch cluster*.

Definition 7. The set of frozen cells that can be traced back to a cell on the straight path from cell z_0 on the j -axis main branch is referred to as a side branch cluster and denoted by $\Theta(z_0)$.

A side branch cluster is a visual notion of a collection of side branches that appear to grow together. Figure 9 shows several side branch clusters and the cells on the corresponding straight path marked with cyan \times . Compared with the straight paths, the deviating paths do not grow very far, because they compete with other straight or deviating paths for vapor accumulation in diffusion. On the other hand, the competition with the deviating paths slows down or may even block the growth of a straight path. When a straight path is blocked, the straight path is a strict subset of the corresponding side branch. This scenario is illustrated in Fig. 10, where three side branches are shown.

The straight path of the middle side branch is blocked by a deviating path of the lower side branch, which grows into a sizable side branch cluster. Through the above definitions one has that if there exists a cell z such that $z \in \Theta(z_0)$ and $z \notin \Phi(z'_0)$, then the paths are nested $\Psi(z'_0) \subset \Phi(z'_0)$. Moreover, the straight path determines the length of the side branch cluster:

Definition 8. Denote by $D(z, z_0)$ the distance between $z_0, z \in \Theta(z_0)$, defined as the smallest number of sites on the lattice between z and z_0 . The length of $\Theta(z_0)$ is

$$D(z_0) := \max_{z \in \Theta(z_0)} D(z, z_0).$$

Through the above definition one can show that there are K cells $z_i \in \Theta(z_0)$ such that the distances satisfy $D(z_i, z_0) = D(z_0)$ for $i = 1, \dots, K$ with $K \geq 2$. Furthermore, there exists

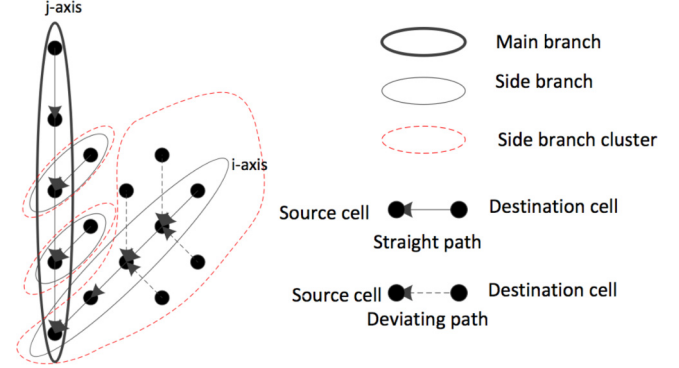


FIG. 10. An arrow linking two cells indicates the source-destination relationship.

$z_i \in \Psi(z_0)$ for $1 \leq i \leq K$, and thus $D(z_0) = F(z_0)$, the length of $\Psi(z_0)$ as in Definition V.

VI. AN ENHANCED REITER'S MODEL

Plates and dendrites are two basic types of regular, symmetrical snowflakes. We observe that while the dendrite images in Figs. 3(a) and 3(b) generated by Reiter's model resemble quite accurately the real snowflake in Fig. 1(a), as seen in Figs. 3(c) and 3(d) and Figs. 1(b) and 1(c), the plate images differ significantly. The plate images in Figs. 3(c) and 3(d) is in effect generated as a very leafy dendrite. One of the reasons that Reiter's model is unable to generate plate images realistically is that the model only includes diffusion, thus not taking into account the effect of local geometry.

As described in Ref. [12], two basic types of mechanisms contribute to the solidification process of snowflakes: diffusion control and interface control. Diffusion control is a nongeometric growth model, where snowflake surfaces are everywhere rough due to diffusion instability, a characteristic result of chaotic dynamics. For example, if a plane snowflake surface develops a small bump, it will have more exposure into the surrounding vapor and grow faster than its immediate neighborhood due to diffusion. Interface control is a geometric mechanism where snowflake growth only depends on local geometry, i.e., curvature related forces. In the small bump example, the surface molecules on the bump with positive curvature have fewer nearest neighbors than do those on a plane surface and are thus more likely to be removed, making the bump move back to the plane. Interface control makes snowflake surfaces smooth and stable, and it is illustrated in Fig. 11.

In summary, snowflake growth is determined by the competition of the destabilizing force (diffusion control) and stabilizing force (interface control). In the absence of interface control, Reiter's model is unable to simulate certain features of snowflake growth.

The interface between the snowflake and vapor regions has potential energy, called surface free energy, due to the unfilled electron orbitals of the surface molecules. The *surface free energy* $\gamma(n)$ as a function of direction n , is determined by the internal structure of the snowflake, and in the case of a lattice plane is proportional to lattice spacing in a given direction.

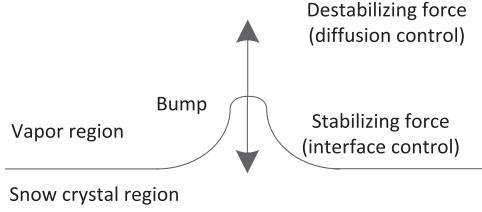


FIG. 11. Two competing forces of diffusion control and interface control that determine snowflake growth, an illustration of the Mullins-Sekerka instability.

Figure 12 plots the surface free energy $\gamma(n)$ of a snowflake as a function of the direction n .

The equilibrium shape of the interface is the one that minimizes the total surface free energy for a given enclosed volume. Wulff construction (see Ref. [12]) can be used to derive the equilibrium crystal shape \mathcal{W}_γ from the surface free energy plot $\gamma(n)$:

$$\mathcal{W}_\gamma := \{r | r \cdot n \leq \gamma(n), \forall n\}. \quad (12)$$

Wulff construction states that the distances of the equilibrium crystal shape from the origin are proportional to their surface free energies per unit area. Figure 12 plots the equilibrium crystal shape of snowflake. Moreover, it shows that due to interface control, snowflake growth is the slowest along the lattice axes, and the fastest along the 30° -offset lattice axes.

This can be explained intuitively. Snowflakes grow by adding layers of molecules to the existing surfaces. The larger the spaces between parallel lattice planes, the faster the growth is in that direction. This effect is completely opposite to the diffusion control we have studied in Sec. IV, where snowflake grows fastest along the lattice axes. This is an example of competition between diffusion control and interface control.

We next propose a new geometric rule to incorporate interface control in Reiter's model. The idea is that the surface free energy minimization forces the lattice points on an equilibrium crystal shape to possess the same amount of vapor so that the surface tends to converge to the equilibrium

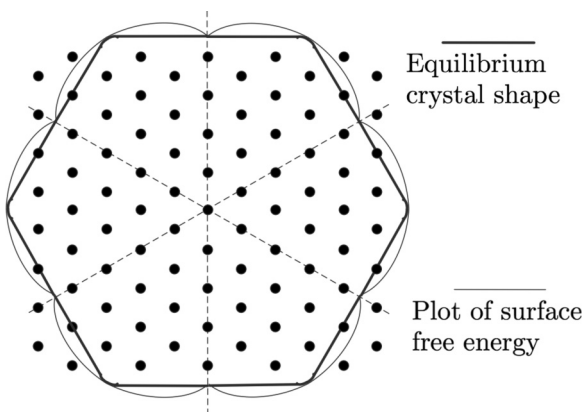


FIG. 12. Surface free energy of snowflake as a function of direction and equilibrium crystal shape of snowflake derived from surface free energy plot with Wulff construction [12].

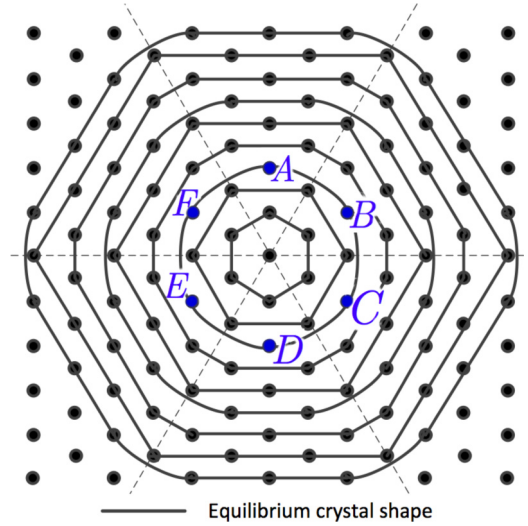


FIG. 13. Equilibrium crystal shape used in the new geometric rule.

crystal shape as the snowflake grows. It should be pointed out that crystals that grow under the control of interfacial kinetic processes tend asymptotically toward a kinetic Wulff shape, the analog of the Wulff shape, except it is based on the anisotropic interfacial kinetic coefficient rather than the anisotropic surface free energy. The proposed model does not take into account the anisotropic interfacial kinetic coefficient based on a lateral motion of steps.

From Fig. 12, we learn that the equilibrium crystal shape is a hexagon except for six narrow regions along the 30° -offset lattice axes where the transition from one edge of the hexagon to another edge is smoothed. The equilibrium crystal shape used in the new geometric rule is shown in Fig. 13.

Figure 13 shows the equilibrium crystal shape used in the new geometric rule and the interface control neighbors of the cells. As an example, cells A, B, C, D, E, F are on the same equilibrium crystal shape. Cells F and B are the interface control neighbors of A , cells A, C are the interface control neighbors of B , etc.

The new geometric rule is applied after Eq. (5): A new variable $\delta_t(z)$ is defined to represent the amount of water to be redistributed for cell z at time t , with initial value $\delta_t(z) = 0$ for all z .

Definition 9. For a given cell z_0 , define two interface control neighbors z_0^1, z_0^2 , which are two neighboring cells of z_0 on the same equilibrium crystal shape.

Define $\bar{s}(z_0)$ as the average of the water amounts in cell z_0 and its two interface control neighbors z_0^1, z_0^2 :

$$\bar{s}(z_0) := \frac{1}{3} [s_{t+1}^-(z_0) + s_{t+1}^-(z_0^1) + s_{t+1}^-(z_0^2)]. \quad (13)$$

For every boundary z_0 , if neither of z_0^1, z_0^2 are frozen, then adjust $\delta_t(z_0)$ as follows:

$$\delta_s(z_0) = \delta_s(z_0) + \varepsilon [\bar{s}(z_0) - s_{t+1}^-(z_0)], \quad (14)$$

$$\delta_s(z_0^1) = \delta_s(z_0^1) + \varepsilon [\bar{s}(z_0) - s_{t+1}^-(z_0^1)], \quad (15)$$

$$\delta_s(z_0^2) = \delta_s(z_0^2) + \varepsilon [\bar{s}(z_0) - s_{t+1}^-(z_0^2)], \quad (16)$$

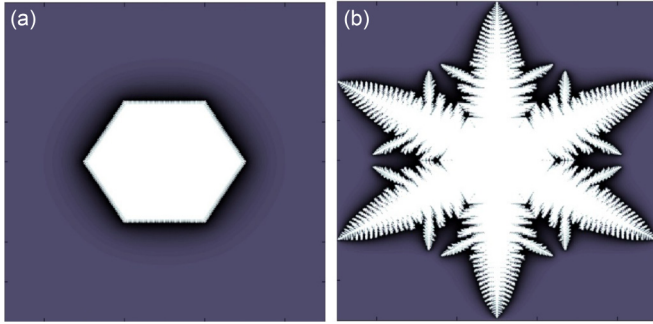


FIG. 14. Snowflake images generated by the enhanced Reiter's model with the new geometric rule, where the variables are (a) $\varepsilon = 0.1$; (b) $\varepsilon = 0.01, \alpha = 1, \beta = 0.4, \gamma = 0.001$.

where $\varepsilon \in \mathbb{R}_{\geq 0}$ determines the amount of interface control. After $\delta_s(z)$ has been adjusted for all z according to Eq. (14)–(16), for every cell z set

$$s_{t+1}^+(z) := s_{t+1}^-(z) + \delta_s(z). \quad (17)$$

Recall that in the original Reiter's model, once water is accumulated in a boundary cell, water stays permanently in that cell. The new function Eq. (17) forces water redistribution particularly among boundary cells to smoothen the snow vapor interface. Figure 14 shows two snowflake images generated by the enhanced Reiter's model with the new geometric rule.

At $\varepsilon = 0.1$, the image above resembles a plate observed in nature much more closely than the ones in Fig. 3. By reducing interface control with $\varepsilon = 0.01$, the snowflake starts as a plate and later becomes a dendrite as diffusion control dominates interface control.

VII. CONCLUSIONS AND FUTURE WORK

In this paper we have analyzed the growth of snowflake images generated by a computer simulation model (Reiter's model [10]) and have proposed ways to improve the model. We have derived an analytical solution of the main branch growth latency and made numerical comparison with simulation results. Subsequently we observed interesting patterns of side branches in terms of growth latency and direction. Finally, to enhance the model, we have introduced a new geometric rule that incorporates interface control, a basic mechanism of the solidification process, which is not present in the original Reiter's model.

The present work has shed light into some interesting patterns that lead to further questions about crystal growth. On the main branch growth, one may ask why the growth latency is almost constant (Fig. 7) and whether this phenomenon is unique to the hexagonal cells or applicable to other two-

dimensional lattices. Concerning the side branch growth, it was noted that some side branches grow much faster than their neighbors, and that with slightly different diffusion parameters the side branch growth latency could change drastically at the same position while the main branch growth latency remains virtually the same. The study in Sec. VI shows that this great sensitivity is attributable to diffusion instability: When the growth of cells in some direction gains initial advantage over their neighbors, the advantage continues to expand such that the growth in that direction becomes even faster. It was noted in Sec. VI that diffusion instability is caused by competition among cells in diffusion, and thus the average number of contributing neighbors is a good indicator to explain diffusion instability. Finally, the enhanced model described in Sec. VI can be used to explore the interplay of diffusion and interface control. For example, one may simulate growth in an environment where the diffusion and interface control parameters vary with time so as to generate images similar to Figs. 1(b) and 1(c).

Recently Reiter's model was used in the study of snowfall retrieval algorithms (e.g., see Refs. [16,17] and references therein), and it was suggested that other mechanisms of snowflake formation from ice crystals besides aggregation must be considered in snowfall retrieval algorithms. It is thus natural to ask whether the enhanced Reiter's model constructed here may provide insights in this direction, as well as when considering crystal growth dynamics as in Ref. [18]. Moreover, since cellular automata models have been considered for numerical computations of pattern formation in snow crystal growth, it would be interesting to analyze the outcome of the implementation of the model presented here to the analysis done in Refs. [13,19].

Finally, the effects of lattice anisotropy coupled to a diffusion process have been studied in Ref. [20] to understand phase diagrams associated to crystal growth. Since this approach seemed useful recently from different perspectives (e.g., see Ref. [21] and references therein), it would be interesting to study the enhanced model constructed here from the perspective of Refs. [20,21].

ACKNOWLEDGMENTS

The research in this paper was conducted by J.L. under the supervision of L.P.S., as part of the Illinois Geometry Lab & MIT-PRIMES program. Both authors are thankful for the opportunity to conduct this research together and would also like to thank K. Libbrecht and N. Goldenfeld for helpful comments. The work of L.P.S. is partially supported by NSF Grant No. DMS-1509693.

- [1] K. G. Libbrecht, The physics of snowflakes, *Rep. Prog. Phys.* **68**, 855 (2005).
- [2] K. G. Libbrecht, A guide to snowflakes, <http://www.its.caltech.edu/~atomic> (2014).
- [3] C. Magono and C. W. Lee, Meteorological classification of natural snowflakes, *J. Faculty Sci., Hokkaido University, Ser. 7, Geophys.* **2**, 321 (1966).

- [4] B. Mason, *The Physics of Clouds* (Oxford University Press, Oxford, 1971).
- [5] U. Nakaya, *Snowflakes: Natural and Artificial* (Harvard University Press, Cambridge, MA, 1954).
- [6] J. Gravner and D. Griffeath, Modeling snowflake growth II: A mesoscopic lattice map with plausible dynamics, *Physica D: Nonlinear Phenom.* **237**, 385 (2008).

- [7] J. Gravner and D. Griffeath, Modeling snowflake growth III: A three-dimensional mesoscopic approach, *Phys. Rev. E* **79**, 011601 (2009).
- [8] C. Ning and C. Reiter, A cellular model for 3-dimensional snowflake growth, *Comput. Graphics* **31**, 668 (2007).
- [9] N. H. Packard, Lattice models for solidification and aggregation, Institute for Advanced Study preprint (1984), reprinted in *Theory and Application of Cellular Automata*, edited by S. Wolfram (World Scientific, Singapore, 1986), pp. 305–310.
- [10] C. Reiter, A local cellular model for snowflake growth, *Chaos Solitons Fractals* **23**, 1111 (2005).
- [11] T. Wittmann and L. Sander, Diffusion-Limited Aggregation, a Kinetic Critical Phenomenon, *Phys. Rev. Lett.* **47**, 1400 (1981).
- [12] J. A. Adam, Flowers of ice beauty, symmetry, and complexity: A review of the snowflake: Winter's secret beauty, *Notices Am. Math. Soc.* **52**, 402 (2005).
- [13] J. W. Barrett, H. Garcke, and R. Nürnberg, Numerical computations of faceted pattern formation in snow crystal growth, *Phys. Rev. E* **86**, 011604 (2012).
- [14] Y. Furukawa, Snow and ice crystal growth, in *Handbook of Crystal Growth*, edited by T. Nishinaga (Elsevier, Amsterdam, 2015), Vol. I, pp. 1061–1012.
- [15] E. Yokoyama, Y. Giga, and P. Rybka, A microscopic time scale approximation to the behavior of the local slope on the faceted surface under a nonuniformity in supersaturation, *Physica D* **237**, 2845 (2008).
- [16] J. Leinonen and D. Moiseev, What do triple-frequency radar signatures reveal about aggregate snowflakes? *J. Geophys. Res. Atmos.* **120**, 229 (2015).
- [17] J. Tyynelä and V. Chandrasekar, Characterizing falling snow using multifrequency dual-polarization measurements, *J. Geophys. Res. Atmos.* **119**, 8268 (2014).
- [18] K. G. Libbrecht, Quantitative modeling of faceted ice crystal growth from water vapor using cellular automata, *J. Comput. Methods Phys.* **2013**, 174806 (2013).
- [19] J. G. Kelly and E. C. Boyer, Physical improvements to a mesoscopic cellular automaton model for three-dimensional snow crystal growth, *Cryst. Growth Des.* **14**, 1392 (2014).
- [20] F. Liu and N. D. Goldenfeld, Generic features of late stage crystal growth, *Phys. Rev. A* **42**, 895 (1990).
- [21] X. Liu, Y. Pu, P. Wang, Z. Dong, Z. Sun, and Y. Hu, Morphological evolution of tridymite crystal in SrO–BaO–Nb₂O₅–CaO–SiO₂–B₂O₃ ferroelectric glass-ceramic, *Mater. Lett.* **128**, 263 (2014).